Check for updates

Thermodynamics of calcined clays used in cementitious binders: origin to service life considerations

Theodore Hanein, [iD] *[a] Hoang Nguyen, [iD] [b] John L. Provis, [iD] [a] Claire Utton[a] and Wolfgang Kunther [iD] [c]

The use of calcined clays in construction materials has attracted significant attention in the last few years. Based on the continued need for sustainable construction to meet global development challenges, the green transition of the cement industry is an urgent necessity. The use of clay-blended cements will keep increasing to meet the need for mass quantities of materials and the prospect of reducing their embodied CO_2, as traditional supplementary cementitious materials are expected to decline in availability. To enable the necessary rapid increase in the fraction of clays that can be used in cements, the use of modeling tools which provide insights into the clays and their reactivity in cementitious systems is of increased interest. The aim is to predict the properties of the calcined clays based on the original rock and calcination conditions, the phase evolution, material properties, and durability of construction materials. This is crucial to reduce the time needed for development and commercialisation, whereas extensive empirical work has been used in the past to achieve material transition in the construction sector, which can be extremely time consuming. This review article therefore aims to provide an overview of available thermodynamic data, issues with database integration, modelling of process parameters, and properties prediction for cementitious materials.

[a]Department of Materials Science & Engineering, University of Sheffield, S1 3JD, Sheffield, UK. E-mail: t.hanein@sheffield.ac.uk

[b]Fibre and Particle Engineering Research Unit, University of Oulu, 90014, Oulu, Finland

[c]Department of Environmental and Resource Engineering, Technical University of Denmark, 2800, Kgs. Lyngby, Denmark

Introduction

The use of calcined clay in cementitious binders is increasing, facilitating the global push towards lower-carbon, sustainable concrete. Global demand for cement exceeds 4 Gt per annum,[1] and assuming a technically plausible replacement level of up to

Dr Theodore Hanein is a UKRI Future Leaders Fellow on Green, Circular, and Smart Cement manufacture. His expertise is mainly in materials thermo-chemistry, and he is Senior Research Fellow (Assoc. Prof.) in the Cements@Sheffield research group in the Department of Materials Science and Engineering at The University of Sheffield as well as Director of the Centre for Experimental Thermodynamics UK. Theo is a member of the Transforming Foundation Industries Future Leaders Group and deputy chair of the RILEM technical committee on upcycling powder minerals into cement matrices.

Dr Hoang Nguyen is a research fellow at Magnesia-based materials and systems team, Fibre and Particle Engineering Research Unit, University of Oulu (Finland). Hoang does research in construction and building materials with more than 10 years of training and experiences in the field. His research interests are low/no-carbon cements, (alternative) cement chemistry, side streams and carbon utilization, and thermodynamic modeling. Hoang's webpage: https://www.oulu.fi/en/researchers/hoang-nguyen.

17920 | *J. Mater. Chem. A*, 2023, **11**, 17920–17937

This journal is © The Royal Society of Chemistry 2023

40% or Portland cement by calcined clay,[2] there is potential market for >1.5 Gt of calcined clay annually in the cement industry alone. Emerging cementitious systems/technologies using calcined clay, such as the limestone-calcined clay–cement blends known as LC[3],[2] have already proven to be suitable for wide scale adoption, based on experimental testing of the cement and concrete performance. However, there is little systematic understanding of how the thermodynamic properties of clays (raw and calcined) and their solid solutions or associated minerals (linked to their origin) will affect the production/calcination process (including interaction with process atmosphere) and their reactivity and performance in cementitious binders. Moreover, the lack of consistency in description of important clay minerals across thermodynamic databases is problematic, and it is necessary to assess and document the availability of thermodynamic data as well as the research gaps in the thermodynamics of calcined clays, to enable full exploitation of the potential of this material.

In the practical application of concrete technology, materials chemistry must be translated to real-life applications, where workers and engineers with little or no chemical background are tasked with manipulating and optimising the multi-phase, multi-step cement hydration reaction process to produce highly durable engineering materials. This field normally relies heavily on empirical solutions for understanding the reactivity and property development of binders, and many important materials are widely used despite an incomplete understanding of their fundamental chemistry. However, the timeframe that is imposed for the green revolution to reach net-zero targets is more ambitious than can be achieved by this style of development in the field of cement and concrete research. Fortunately, the advancement of computing technology/power makes thermodynamic calculations much more accessible, and potentially also sufficiently user-friendly to enable their direct use in cementitious materials design.[3,4]

The application of thermodynamic principles to the study of cement chemistry was pioneered by Le Chatelier in the early 20th century,[5] and thermodynamic analysis has since been applied to almost all aspects of cement science, particularly in the last two decades.[6–8] On the other hand, clays are fine-particulate (<20 μm) weathering products of silicate bearing rocks whose constituents depend on the host rock/deposit and climatic conditions. Weathering can occur locally and produce relatively pure clays, but is often combined with erosion and transport processes, which leads to clay deposits that are then sedimentary in nature and yield combinations of clay minerals, such as kaolinite (1 : 1 clay) and illite (2 : 1 clay), in addition to other, non-clay, associated minerals. It is therefore timely to collect the available data and approaches used in calcined clays and calcined clay–cement binders, ranging from the raw materials to the calcination process[9] and the hydration and durability of the binders: from origin to service life. This will enhance utilisation and understanding of the different models and approaches that will lead to reduced design periods and faster translation to commercial products.

John Provis is Professor of Cement Materials Science and Engineering at the University of Sheffield, UK. He completed a PhD in Chemical Engineering at the University of Melbourne in 2006, and since then has developed a research programme to investigate the fundamental science and applications of innovative cements. He is Editor-in-Chief of the RILEM flagship journal Materials and Structures, an ERC StG grantee, was the 2013 RILEM Robert L'Hermite Medallist, is a Fellow of IoM3, ACerS, RILEM and ICT, has supervised more than 80 doctoral and postdoctoral researchers, and has published over 300 journal articles.

Dr Claire Utton is a research fellow at the University of Sheffield in the Department of Materials Science and Engineering. Claire's research is focused on the development of materials which can withstand extreme environments, such as refractory alloys for gas turbine engines or materials for use in fusion or fission reactors. She has over 10 years' experience of thermodynamic modeling, including the CALPHAD method for thermodynamic database development and of experimental determination of phase diagrams.

Dr Wolfgang Kunther is a material researcher with a background in civil engineering and concrete technology, who works as Assoc. Professor at the Department of Environmental and Resource Engineering of the Technical University of Denmark. His research encompasses the chemistry of cement in connection with supplementary cementitious materials, such as calcined clays, and the deterioration of these materials when exposed to salty solutions. He often uses a combination of experimental methods and thermodynamic modeling to support the investigations, especially where measurements are not (yet) feasible.

This journal is © The Royal Society of Chemistry 2023

J. Mater. Chem. A, 2023, **11**, 17920–17937 | **17921**

To be able to predict and understand the behaviour of these complex materials when exposed to certain environments, we will start by discussing the different ideal minerals, to describe their (thermo)chemistry and compositional variability that would represent real-life clays that will be used in blended cement production, which may be either quite pure or relatively impure. It is noted that alkali-activation is another (potentially very attractive) pathway to the production of clay-based cementitious binders,[10–12] but is deemed to be beyond the scope of the current review, which is instead focused on blends with Portland cement. The review will include a description of calcination process modeling and the aspects that can be influenced to control and optimise the process. Finally, a review of modeling approaches for the hydration, pozzolanic reactions, and durability of binary and ternary binders, including limestone fines, will be presented.

Survey of related thermodynamic data of raw clays

Due to the varying chemical nature of clays, it is not straightforward to derive and exploit thermodynamic data of clay minerals; nonetheless, some useful data sets do exist. Here, we performed a survey to provide an overview about the consistency and comparability of several of the most common and well-known thermodynamic databases. These datasets are shown in Table 1; for each, we have calculated and compared the solubility constants of various clays (following reaction and species shown in Table 2) as a function of temperature.

Fig. 1 shows the comparison between $\log K$ and temperature among the surveyed databases for 1 : 1 (Fig. 1a and b) and 2 : 1 clays (Fig. 1c–e). Overall, there is a good consistency among databases for kaolinite, halloysite, and pyrophyllite. For illite (Fig. 1c), the Thermoddem[17,18] and PHREEQC[14] databases exhibit a mismatch with higher $\log K$ values in a temperature range of 0–100 °C compared to the other databases. In contrast, smectite shows a high variation in its thermodynamic properties due to the solid solution nature of the clay. The high Fe and Mg content are in a proportional relation with the $\log K$ of the clay, while the high content of chemically bound water in the smectite structure correlates with decreasing solubility constants. Therefore, there are several solid solution models

Table 2 Species used to calculate $\log K$ for each clay minerals based on the selected thermodynamic databases

Clay mineral	Species
Kaolinite	H^+; Al^{3+}; $SiO_{2(aq)}$; H_2O
Halloysite	H^+; Al^{3+}; $SiO_{2(aq)}$; H_2O
Illite	H^+; Mg^{2+}; K^+; Al^{3+}; Fe^{2+}; $SiO_{2(aq)}$; H_2O
Pyrophyllite	H^+; Al^{3+}; $SiO_{2(aq)}$; H_2O
Smectite	H^+; Mg^{2+}; Na^+; K^+; Al^{3+}; Fe^{3+}; Fe^{2+}; $SiO_{2(aq)}$; H_2O

established in the literature to predict the thermodynamic properties of these clays.

There are two models of solid solutions for clay minerals that are known in the literature. First is the ideal solid solution model proposed by Tardy and Fritz,[24] which proposed that the component activities are assumed to be controlled by ideal mixing of end-member components.[24,25] This is described via eqn (1):[24]

$$\log K = \sum_{i=1}^{i=n} X_i \log K_i + \sum_{i=1}^{i=n} X_i \log X_i \qquad (1)$$

where X is mole fraction of an end-member and i is the number of end-members in the solid solution. The second model was proposed by Aagaard[26] and further developed by Giggenbach,[27] and considers that the solid solution was created by ideal site mixing of individual atoms occupying the clay mineral's interlayer, octahedral, and tetrahedral sites. Therefore, the activity of a solid solution can be calculated by eqn (2):[27]

$$a_i = k_i \prod_s \prod_j X_{j,s}^{\theta_{j,s}} \qquad (2)$$

where k_i is a constant relating the inter- and intra- crystalline standard states for the ith component; $X_{j,s}$ is the mole fraction of the jth atom on the sth site in one mole of the ith thermodynamic component; $\theta_{j,s}$ is the stoichiometric number of sites occupied by the jth atom. In addition, only for a perfectly ordered component is $k_i = 1$.

To illustrate this, we take an example from the difference between pyrophyllite and smectite, where pyrophyllite is a pure end-member of aluminosilicate in the smectite group.[28] Smectite is a group of 2 : 1 phyllosilicates with a total layer charge between 0.2 and 0.6 (negative) per half unit cell. The group can

Table 1 Selected thermodynamic databases containing information for the main clay minerals

Databases	Temperature range (°C)	$\log K$ calculation	References
Minteq	0–100	Van't Hoff equation	13
PHREEQC	0–100	Van't Hoff equation	14
Lawrence Livermore National Laboratory (LLNL)	0–300	Van't Hoff equation	15
Yucca Mountain project	0–300	Van't Hoff equation	16
Thermoddem	0–300	Polynomial	17 and 18
Thermochimie	0–300	Polynomial	19 and 20
NEA	—	Polynomial	21
JAEA	—	SUPCRT	22
Holland and Powell	—	—	23

17922 | *J. Mater. Chem. A*, 2023, **11**, 17920–17937

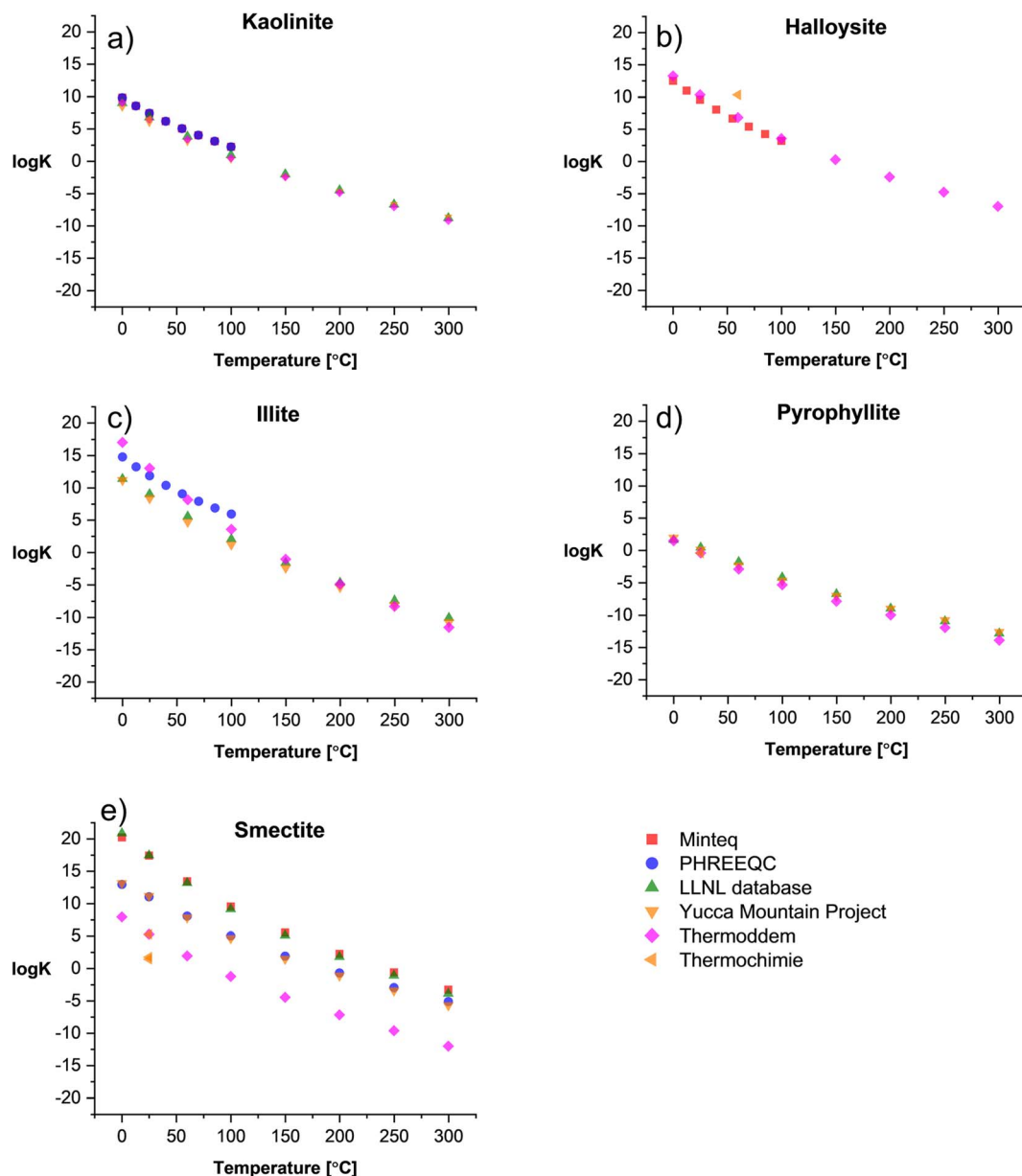This journal is © The Royal Society of Chemistry 2023

Fig. 1 log *K* vs. temperature of selected (a and b) 1 : 1 clays and (c−e) 2 : 1 clays summarized from existing TDBs.

be classified according to the following criteria (1) dioctahedral or trioctahedral layer, (2) octahedral chemical composition, and (3) density and location of layer charge.[28] Hence, a wide range of cations can populate sites in the smectite structure. Like other members in the smectite group, pyrophyllite has a 2 : 1 layered structure with an ideal structural formula of $Al_2Si_4O_{10}(OH)_2$. The phase is known to have three different layer stacking orders: (1) a two-layer monoclinic (2M), (2) a one-layer triclinic (1Tc), and (3) a disordered form.[29] The dehydroxylation of the clay occurs between 500 and 900 °C,[9,30] which in turn, gives rise to five-coordinated Al, forming distorted trigonal bipyramidal AlO_5 units in the octahedral sheet.[31] At 1000 °C, the tetrahedral sheet breaks down and leads to a partial segregation of amorphous SiO_2.[32]

Fig. 2a shows the formation of trioctahedral and dioctahedral solid-solutions based on their ranges of composition compared to the pure member, while Fig. 2b presents the dehydration model of smectite driven by temperature or water activity. Vidal and Dubacq[33] then estimated the $V°$, $S°$ and $C_p(T)$ of all of the dehydrated end-members defined in Fig. 2 using oxide summation techniques. The formation enthalpy was also calculated to be in-line with the experimental data at 1 bar and 25 °C, to ensure the stability of hydrated smectite instead of mica and aluminosilicate at low temperature, and reproduce the observations of smectite–illite equilibrium, as well as vermiculite or mica segregation observed with increasing temperature in the experiments and in nature.[33]
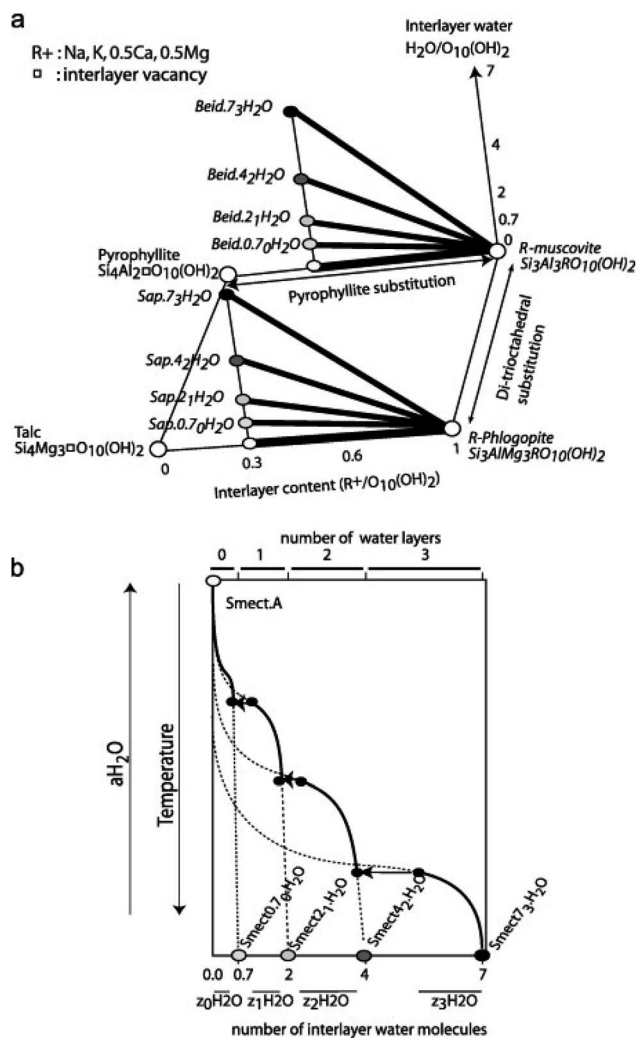
Fig. 2 Schematic representation of the solid solution models. (a) The thick lines show the ranges of composition covered by the tri-octahedral and dioctahedral solid-solution models and the end-member compositions are in italics in which Beid = beidellite and Sap = saponite. (b) Dehydration model of smectite with temperature or water activity. The water content of the end-members is shown by the circles on the lower horizontal axis. The continuous and dashed lines indicate the stable and metastable parts of the four solid solutions between Smectmn H_2O and Smect A. The ranges of interlayer water content for the Smect with 0–3 interlayer water are indicated by $z0H_2O$ to $z3H_2O$. The transitions from nw to $(n-1)$w occur at discrete values of temperature or aH_2O, and are shown by the horizontal arrows. Reproduced from ref. 33 with permission from Elsevier, copyright 2009.

Recently, Blanc *et al.*[34] introduced a computing tool, named ClayTherm (see Fig. 3), to estimate the thermodynamic properties of clay minerals as well as ISTherm dedicated to deriving illite/smectite compositions. The tool uses the thermodynamic properties of ions from Thermochimie[19] and Thermoddem[17] databases and advances from merging the model of Blanc *et al.*[35] for the anhydrous clays and the Gailhanou *et al.*[36] and Vieillard *et al.*[37] models for the hydration of clays. The model has capability to predict the equilibrium constants of clay

minerals and compare the calculated thermodynamic properties to the solubility data selected from the literature.

To further assess the reliability of these databases for the clay minerals, the standard entropies retrieved from these datasets were compared to the estimated standard entropy based on the clay's formula unit volume as proposed by Jenkins and Glasser[38] and used for cement minerals by Ghazizadeh *et al.*[8]. Those authors identified that the standard molar entropy of inorganic phases not containing discrete water of hydration (*i.e.*, in this context, clay minerals with bound hydroxyl groups but no molecular water) can be correlated with the formula unit volume as follows:

$$S_{298}^0 = 1262 \times V_m + 13 \quad (3)$$

where V_m (nm³ per formula unit) is the formula unit volume which can be obtained from the molar volume V_{molar} (nm³ mol⁻¹) *via* the following equation:

$$V_m = V_{molar} \times \frac{10^{21}}{NA} \quad (4)$$

where NA is the Avogadro constant (6.022×10^{23} mol⁻¹). Fig. 4 shows the reported standard entropy of clays in the databases compared to the estimated values. All the entropies are well in line with the estimation, noting that the Jenkins and Glasser estimation had a quoted ±12.6% uncertainty when applied to their larger data set. Hence, the linear equation proposed in ref. 38 is a reliable tool to predict the standard entropy of clays and their solid solutions.

The heat capacity (C_p) of clay minerals is temperature dependent and can often be measured *via* experiments. Here, we evaluate the empirical Neumann–Kopp (NK) rule to estimate heat capacity of clays. The NK rule[39,40] was described as: "Each element (in the solid state) has essentially the same specific or atomic heat in compounds as it has in the free state". The rule can be expressed as the following equation:

$$C_p(A_aB_bC_{c(s)}) = aC_p(A_{(s)}) + bC_p(B_{(s)}) + cC_p(C_{(s)}) \quad (5)$$

where the solid $A_aB_bC_c$ is a composition of solid elements A, B, and C *via* the following reaction:

$$aA_{(s)} + bB_{(s)} + cC_{(s)} = A_aB_bC_{c(s)}. \quad (6)$$

The estimated C_p from the NK rule is then compared with the $C_p = f(T)$ function:[41] $C_p = A_1 + A_2 \times T + A_3 \times T^{-2} + A_4 \times T^{-0.5} + A_5 \times T^2$. The temperature range and coefficients of kaolinite (1 : 1 clay), pyrophyllite (2 : 1 clay), and relevant oxides are shown in Table 3 (extracted from ref. 41).

Fig. 5 shows very good agreement between the two approaches to obtain the heat capacity of both 1 : 1 and 2 : 1 clays. Hence, the NK rule can reliably estimate the C_p value of the clays based on their stoichiometry. Note that the NK rule is applicable in the reported range of temperature (*i.e.*, 298–800 K) for clays; however, there may be a need to adjust the estimated C_p considering the contribution of other factors such as the variation of thermal expansion and compressibility at high temperature, beside the lattice vibrations and dilation.[39,42]

17924 | *J. Mater. Chem. A*, 2023, **11**, 17920–17937

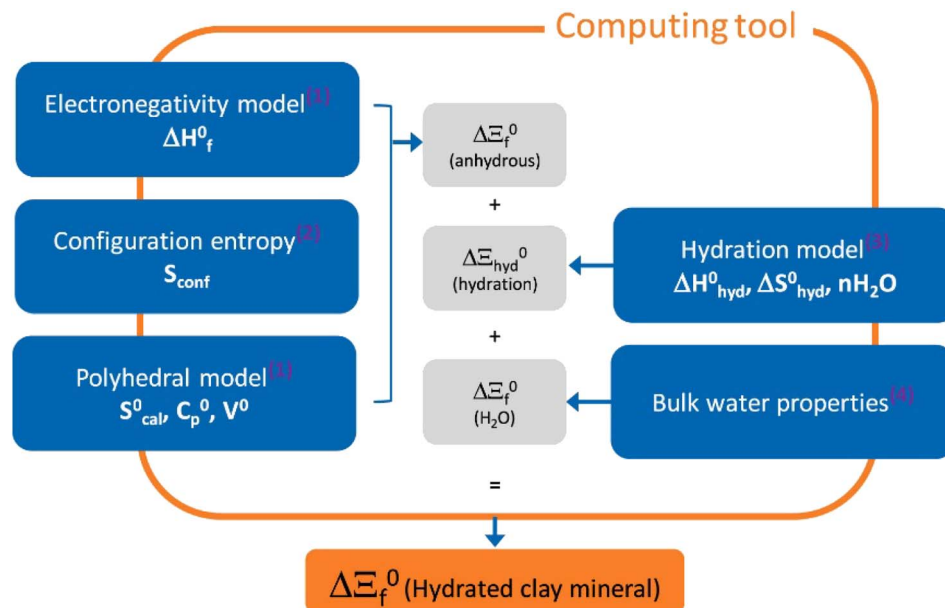This journal is © The Royal Society of Chemistry 2023

Fig. 3 The overall approach of ClayTherm to provide thermodynamic properties for hydrated clay minerals. Reproduced from ref. 34 with permission from Elsevier, copyright 2021.
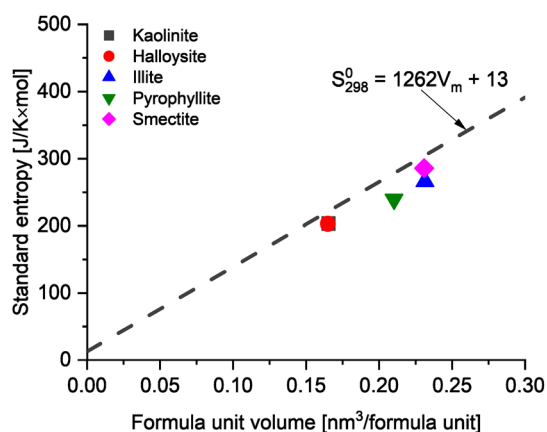

Fig. 4 The comparison between data from thermodynamic databases and estimated values of standard molar entropy based on the formula unit volume[38] of common clays.

Clay calcination and process atmosphere

The favourable pozzolanic properties of calcined clays can be generated through calcination of the clay under specific conditions to achieve maximum dehydroxylation while avoiding sintering and recrystallisation. Various clay types can be dehydroxylated to produce supplementary cementitious materials (SCMs),† and the most studied is kaolinite, which forms metakaolin when calcined. The ideal calcination temperatures of kaolinite-rich clay reported in the literature vary and are usually

reported as a range, depending largely on process conditions (it is a kinetically controlled process[43]) as well as the degree of disorder (e.g. layer stacking faults) within the clay itself, and associated minerals within the clay.[9] For example, calcium carbonate can decompose at clay calcination temperatures and undesirably further react with the aluminosilicate; thus negatively influencing the mineralogy of the final calcined clay product.[44] Conversely, the CaO content of calcined marl is sometimes considered to be beneficial to boost its pozzolanic properties[45,46]
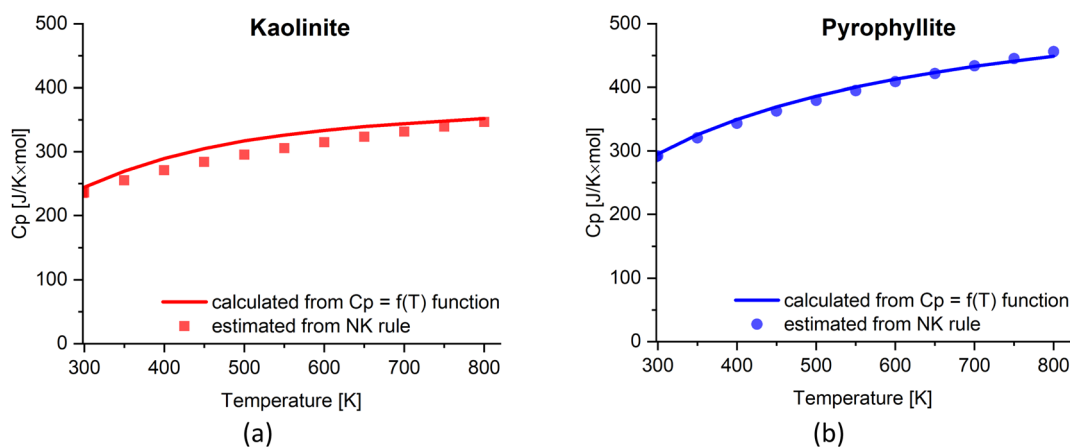
The dehydroxylation of clay minerals is the key reaction in clay calcination from a thermodynamic point of view. The dehydroxylation temperature of clays such as kaolinite ($Al_2Si_2O_5(OH)_4$), illite (e.g., $K_{0.65}Al_2[Al_{0.65}Si_{3.35}O_{10}](OH)_2$), or montmorillonite (e.g., $Ca_{0.33}Al_2Si_4O_{10}(OH)_2 \cdot nH_2O$) will change depending on the H_2O partial pressure of the process atmosphere. Atmospheric control has been shown to be a critical aspect in cement clinker calcination[7,47,48] and the same phenomenon is at play during the calcination of clays. Considering the reaction $Al_2Si_2O_5(OH)_4 \rightarrow Al_2Si_2O_7 + 2H_2O\uparrow$, applying Le Chatelier's principle, the increase of water vapour pressure in the system will shift the equilibrium to the left (Fig. 7). In a production process, this implies that the formation temperature (and energy demand) of metakaolin will increase with increasing H_2O partial pressure. The atmospheric composition and H_2O partial pressure can vary greatly depending on the process configuration and fuel used for clay calcination. The H_2O partial pressure can vary between 1% and $\sim$100% depending on the fuel and oxidant (see Appendix).

The thermodynamic data for kaolinite and metakaolin are taken from ref. 49 while the data for H_2O are taken from ref. 50. These data are used to calculate the dehydroxylation

† It must be noted that mechanochemical processes are also possible to dehydroxylate/activate clay, but are beyond the scope of this discussion.

This journal is © The Royal Society of Chemistry 2023

J. Mater. Chem. A, 2023, 11, 17920–17937 | 17925

Table 3 The coefficients of clays and oxides in the defined range of temperature

Clay	Formula	A_1	A_2	A_3	A_4	A_5	Temp. range [K]
Kaolinite	$Al_2Si_2O_5(OH)_4$	1430.3	-7.885×10^{-1}	8.334×10^6	-1.852×10^4	3.034×10^{-4}	298–800
Pyrophyllite	$Al_2Si_4O_{10}(OH)_2$	746.8	-5.345×10^{-2}	—	-7.578×10^3	1.986×10^{-5}	298–800
Oxide							
Al_2O_3		161.2	-1.352×10^{-3}	-1.815×10^6	-1.059×10^3	5.381×10^{-7}	298–2250
SiO_2		81.145	1.828×10^{-2}	-1.81×10^5	-6.985×10^2	5.406×10^{-6}	298–884
H_2O (ideal gas)		27.057	1.7584×10^{-2}	2.7696×10^5	-2.766×10^1	-2.509×10^{-6}	298–2500

Fig. 5 The estimated C_p value of (a) kaolinite and (b) pyrophyllite based on NK rule compared with the $C_p = f(T)$ function.[41]

temperature of kaolinite over a range of H_2O partial pressures as shown in Fig. 6. It is shown that the dehydroxylation temperature of kaolinite changes from 525 °C when H_2O vapour pressure is 1%, to 605 °C at 10%, and 695 °C at 100%. Calcination

Fig. 6 Thermodynamic dehydroxylation temperatures of kaolinite to metakaolin at various H_2O partial pressures where the thermodynamic data for kaolinite and metakaolin are taken from ref. 49 while the data for H_2O are taken from ref. 50.

under vacuum may also result in dehydroxylation temperatures as low as 300 °C (although this still needs to be tested experimentally). These variations in calcination temperatures will influence the kinetics of calcination as well as the rigidity of microstructure of the produced clay, and thus also the clay reactivity. At higher temperatures, the thermodynamically most stable transformation of metakaolin yields mullite and crystalline SiO_2 at 980 °C (ref. 49) with low reactivity in cementitious binders. The influence of H_2O partial pressure on the conversion of kaolinite to metakaolin has also recently been assessed through density functional theory[51] and the results are in reasonable agreement.

Thermodynamic data, up to 1000 K, for kaolinite is taken from ref. 52 and now compared with the data in ref. 49; it is shown that there is a rather large difference in kaolinite enthalpy and Gibbs energy between the two as shown in Fig. 7. Data for andalusite, mullite, and quartz form ref. 52 are also plotted in Fig. 7; it is shown that kaolinite is only thermodynamically stable up to 400 K and 1 bar total pressure. Furthermore, metakaolin is never thermodynamically stable, even if the data are shifted downwards to coincide with the Haas data at known dehydroxylation temperatures. Metakaolin is indeed a metastable phase and more experimental tests are needed to understand the series of reactions that may occur during service life[53] (in the context of blended cement/concrete) in the presence of various phases/ions in solution over time which can link to the durability of the binder.
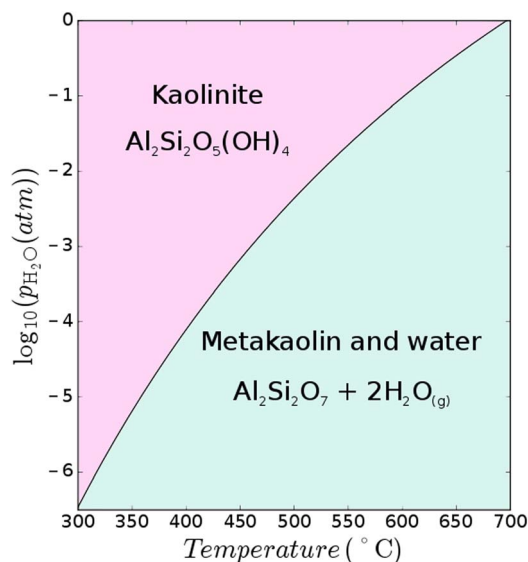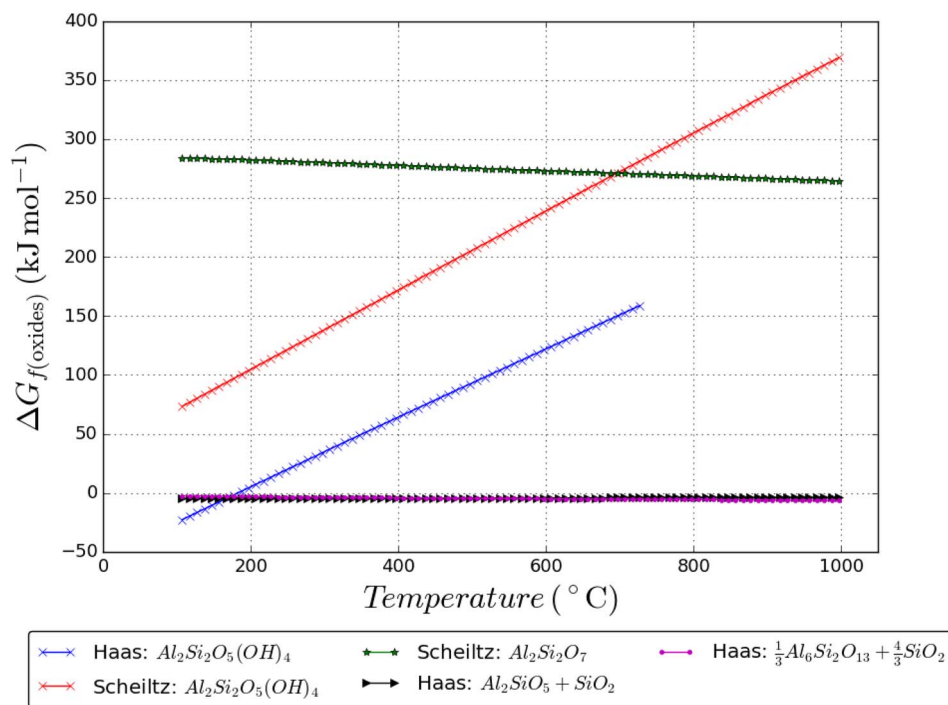
17926 | J. Mater. Chem. A, 2023, 11, 17920–17937

This journal is © The Royal Society of Chemistry 2023

Fig. 7 Gibbs energy of formation from the oxides of various sets of phases, showing the thermodynamically stable products. Where H_2O gas forms, the pressure is set at 1 bar. Haas = ref. 52 and Schieltz = ref. 49.

Other solid–gas interactions: CO_2, O_2, SO_2, and halogens

The CO_2 in the process atmosphere could have a significant role on the calcination of clays. $CaCO_3$ formation as function of CO_2 partial pressure is shown in Fig. 8, plotted alongside the kaolinite–metakaolin conversion temperatures previously discussed; both H_2O and CO_2 are major components of fossil fuel combustion and H_2O is the major product of hydrogen

Fig. 8 Superimposed plots of kaolinite dehydroxylation and calcium carbonate calcination at various H_2O and CO_2 partial pressures respectively.

combustion. Fig. 8 may be taken as a useful guide, locating a "Goldilocks zone" for manufacturing of calcined clay in various fuels, but kinetic factors will also need to be considered.

On the other hand, for clay minerals containing calcium, sodium, and potassium (e.g., montmorillonite and muscovite), the CO_2 may also play an important role. Under the conditions used for clay calcination, $CaCO_3$, Na_2CO_3, and K_2CO_3 are stable; therefore, depending on the CO_2 concentration, the clays may interact with the CO_2 to form carbonates along with aluminosilicates during calcination. However, this will need to be confirmed via experiments. Any segregation of Ca, Na, and K from the clay minerals may also have a significant effect on the clay reactivity.

Sulfur-containing minerals such as pyrite and alunite are found in clay while sulfur is also usually found in the process atmosphere, originating from the combustion of sour fossil fuels, and depending on the fuel used. SO_2 concentration in kilns can range from 100–3000 ppm depending on the fuel properties. The reactions that SO_2 can undergo greatly depend on whether the atmosphere is oxidizing (contains O_2). Several sulfate compounds may form through the process but they require oxygen gas ($SO_2 + \frac{1}{2}O_2 \rightarrow SO_3$); furthermore, the breakdown of sulfur containing compounds may also be influenced in the presence/absence of sulfur. Halogen concentrations in calcined clay manufacture may also fluctuate. Depending on fuels used, combustion can introduce halogens into the product through the process atmosphere. Information on the effect of halogens on clay quality is scarce and require further investigation. It is unclear whether these are going to be important at the very low levels that will be found in a practical
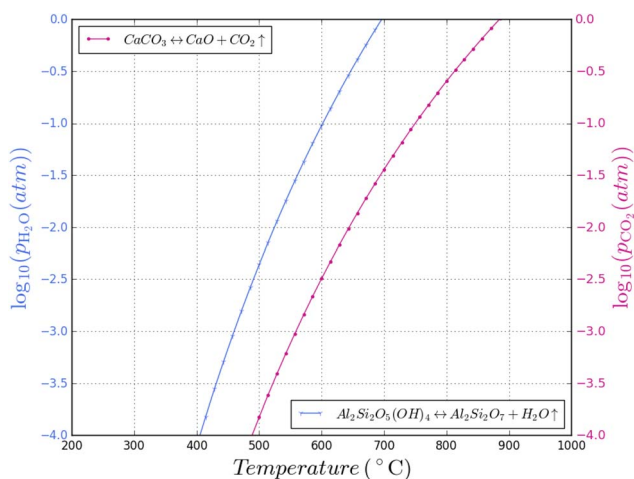
This journal is © The Royal Society of Chemistry 2023

J. Mater. Chem. A, 2023, **11**, 17920–17937 | **17927**

process; however, in summary, it is important to study the solid gas reactions in clay calcination and thermodynamics can be used here as an important tool.

Clay conversion (forced weathering and diagenesis)

Clay minerals form naturally during the weathering of common rock-forming silicates.[54] In nature, clays form as a product of the interaction of silicates and water at ambient or near-ambient conditions in which the minerals slowly accumulate at or near the surface of rocks exposed to atmosphere or in the shallow subsurface. The weathering conditions strongly influence the formation of different clay minerals. A relatively low pH combined with a moderate silica activity and low amounts of (earth)-alkalis are favourable to form kaolinite.[55] Therefore, kaolinite is often deposited in tropical soils where the climate (*e.g.*, rainfall and high heat) coupled with organic matter causes extensive leaching of alkali and earth-alkali metals; there are numerous weathering pathways that can lead to the formation of kaolinite.[56,57] In contrast, kaolinite is much less abundant in cooler and dry regions. In such climates, other clay minerals such as illite and chlorite are more dominant as weathering products in soils.[57] It follows that hydrothermal conversion of clay is also possible, mimicking the weathering process in nature for clay formation. The formation of clay minerals can be also accelerated in hydrothermal conditions by alteration of aluminosilicate parent rocks.

It may also theoretically be possible to interconvert between different clay structures. A thermodynamic assessment using data from Haas Jr *et al.*[52] and the model constructed by Hanein *et al.*[7] was used to assess the difference in Gibbs free energy of the reaction $Al_2(OH)_2Si_4O_{10} + H_2O \rightarrow Al_2Si_2O_5(OH)_4 + 2SiO_2$ at
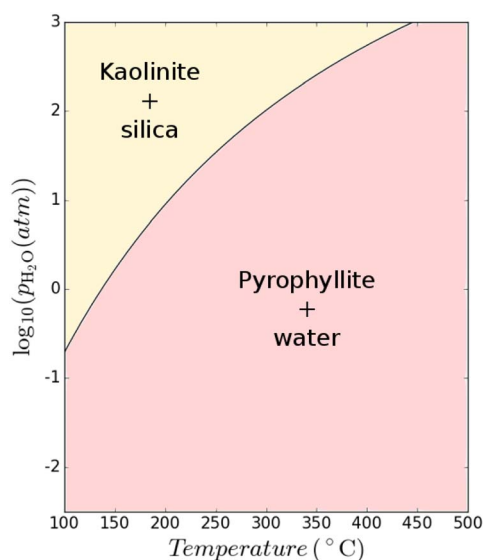

Fig. 9 Thermodynamic calculations showing the possibility of converting 2 : 1 clay to 1 : 1 clay at various temperature and H_2O partial pressure conditions.

varying temperatures and H_2O partial pressures as shown in Fig. 9. The possibility to convert 2 : 1 clays to 1 : 1 clays, by reacting only with water, is thus revealed by our critical assessment of existing data; however, a fully consistent thermodynamic database must be used and validated and further research will be needed to verify and optimize the conditions of accelerating the formation of 1 : 1 clays of higher cementitious value *via* low-energy processes.

Transformation of iron oxides for colour control

The aspect/colour of calcined clay is a significant factor that can restrict usage.[58] Most low-grade kaolinitic clays contain Fe that is often present in hydrous forms ($Fe(OH)_3$ or $FeOOH$) in clays that decomposed to form significant amounts of hematite (Fe_2O_3), greater than a few wt%. Depending on the iron content and oxygen availability, the material is red after calcination, which can be undesirable in the industrial use of cement product. There are four iron oxide minerals as shown in Table 4. There is a change in the oxidation state of iron in reducing atmosphere: hematite (Fe_2O_3) – magnetite (Fe_3O_4) – wüstite (FeO) – iron (Fe). The equilibrium stability ranges depend on temperature and partial pressure of oxygen (P_{O_2}). The calculated phase diagram (T-P_{O_2}) is shown in Fig. 10. Magnetite converts to hematite even in reducing atmospheres at low temperatures.

Martirena *et al.*[58] discuss the mechanisms involved in the colour of the final clay product. Stabilisation of magnetite at low temperature is required to avoid the red colour associated with hematite and produce calcined clay with the same gray colour as traditional cement. It is shown that the oxidation states of the final oxides are the key indicator of colour and that the colour can be controlled by maintaining sufficiently reducing conditions upon cooling of the clay, *i.e.*, starving the atmosphere of oxygen by adding oxygen scavengers. However, the transformation to hematite is a naturally occurring process, and whether these reactions will occur in the concrete placed in environments where oxygen is readily available is still not known.

It is not discussed in the cement-related literature, how thermodynamics can play a crucial role in stabilising colour, simply by the introduction of dopants or inorganic modifiers that will enable enhanced thermodynamic stability of magnetite to lower temperatures without the need for an oxygen scavenger. It should be noted that the degree of reducing environment is crucial – systems with an oxygen scavenger (*e.g.*, C or CO) differ from inert atmospheres of nitrogen or argon normally found in laboratory furnaces. Some data of the effects of substitutional elements on magnetite–maghemite and maghemite–hematite transition temperatures are available in the literature.[60,61] Thermodynamic data to model iron oxide solid solutions are also available for a number of substitutional elements in *e.g.*, Factsage or Thermo-Calc Software databases.

Using Thermo-Calc software and TCOX Metal Slag and Oxides Database version 11,[59] the effect of elements Cr, Mn, Al,

17928 | *J. Mater. Chem. A*, 2023, **11**, 17920–17937

This journal is © The Royal Society of Chemistry 2023

Table 4 Iron oxide mineral information

Mineral name	Chemical formula	Oxidation state of Fe	Crystal structure	Colour
Wüstite	FeO	2+	Cubic/halite	Black
Magnetite	Fe_3O_4	2+, 3+	Cubic/spinel	Black
Maghemite	$\gamma\text{-}Fe_2O_3$	3+	Cubic with a tetragonal supercell/spinel	Brown
Hematite	$\alpha\text{-}Fe_2O_3$	3+	Trigonal/corundum/Al_2O_3	Red

Ni and Mg on stability of Fe-oxides was calculated. The database was validated by comparing calculated phases diagram at various P_{O_2} values and temperatures with published literature where available, which showed good agreement for these elements.

At $P_{O_2} = 0.21$ (partial pressure of oxygen in earth's atmosphere) undoped magnetite is calculated to be stable between 1384–1594 °C. Adding Mg stabilises magnetite to temperatures below 1384 °C (Fig. 11). The maximum solubility of Mg in magnetite is calculated to be 0.14 mole Mg. The phase diagram predicts the single-phase region of magnetite to be narrow below approximately 750 °C to room temperature. When the mole fraction of Mg is increased above 0.14, both periclase (MgO) and magnetite are stable to low temperatures. Periclase has a relatively high solubility for Fe at high temperatures (max. solubility ~0.26 mole fraction Fe at 1735 °C) but as temperature decreases the solubility of Fe also decreases significantly. It must be noted however that there is no predicted solubility of Mg in hematite, and therefore a two-phase region of hematite and magnetite exists as soon as Mg is added below 1384 °C. Our calculated phase diagram is in agreement with reported data.[62]
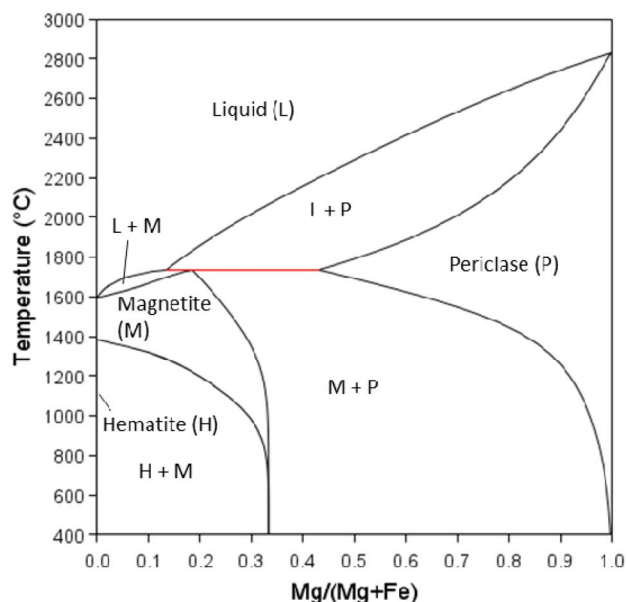

Fig. 11 Fe–Mg–O pseudo binary phase diagram between 'Fe₂O₃' and MgO for $P(O_2)$ gas = 0.21 calculated using Thermo-Calc software (TCOX Metal Slag and Oxides Database version 11) where M = magnetite (Fe,Mg)₃O₄, H = hematite (Fe₂O₃), P = periclase (Fe,Mg)O.
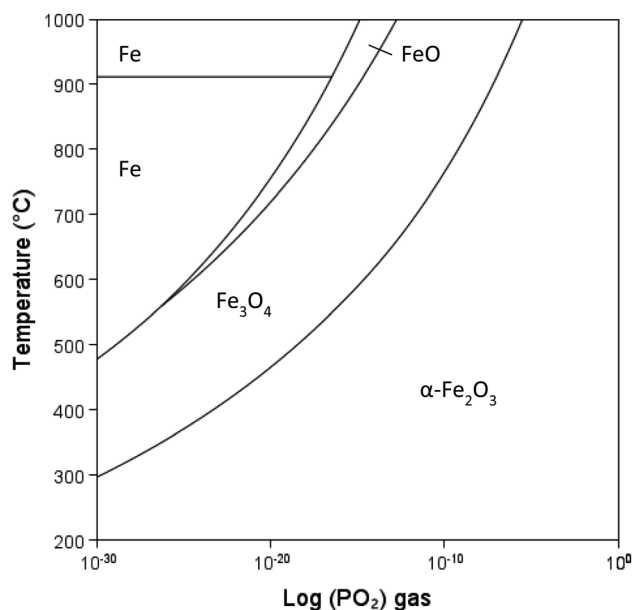
Fig. 12 shows change in stability of magnetite (single phase region) with additions of elements: Mg, Ni, Cr, Mn or Al. The transition temperature for a given composition was calculated for $P_{O_2} = 0.21$. Al and Cr stabilise magnetite at higher temperatures, increasing the transformation temperature above 1384 °C. Mn reduces the transformation temperature, but Mn substituted magnetite is not stable below 954 °C. In contrast, Ni and Mg were calculated to stabilise magnetite at room temperature.

The partial pressure of O_2 as well as temperature can aid in stabilising the magnetite to lower temperatures as indicated in Fig. 13. P_{O_2} vs. composition plots are calculated for temperatures of 1200, 1000, 800, and 600 °C for Mg substitution. The single-phase magnetite region is stable to lower temperatures when decreasing P_{O_2}. Increasing Mg content extends the single-phase magnetite region to higher P_{O_2} values. The two-phase periclase – magnetite region, however, is stable over a wider range of temperature and P_{O_2} range. Although the Mg is calculated to stabilise magnetite to low temperatures, it is still not certain whether these equilibrium phases will form under real-life calcination conditions and further experiments are required.
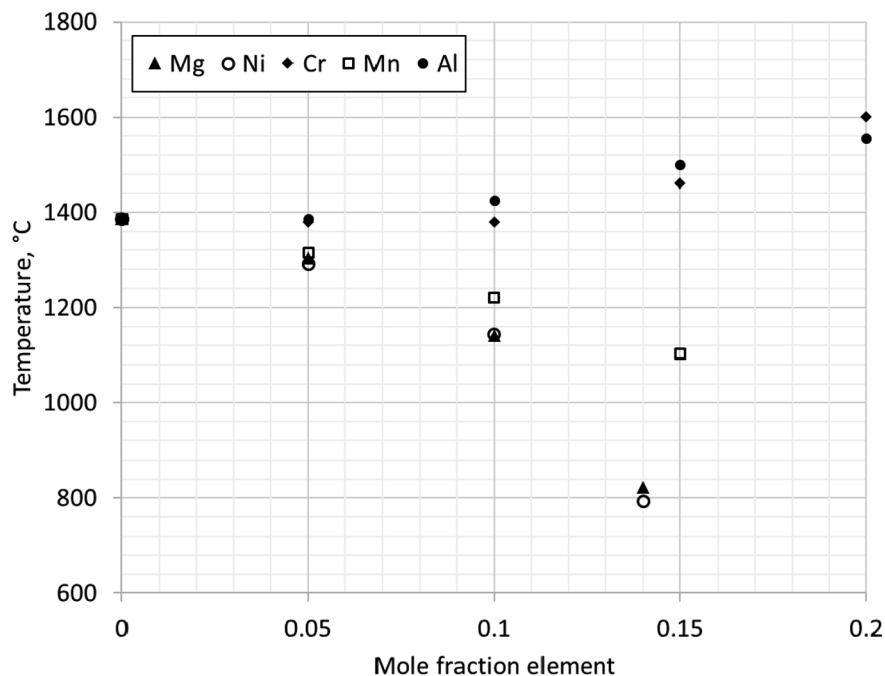

Fig. 10 Fe–FeO–Fe₃O₄–Fe₂O₃ stability diagram with changing temperature and P_{O_2} gas, calculated using Thermo-Calc software (2022b) and TCOX Metal Slag and Oxides Database version 11.[59]

Fig. 12 Change in stability of magnetite (single phase region) with additions of elements Mg, Ni, Cr, Mn or Al. Points indicate minimum temperature at which single phase magnetite is stable for given substitution calculated using Thermo-Calc software TCOX Metal Slag and Oxides Database version 11.

Using *ab initio* calculations

Theoretical chemical methods including density functional theory (DFT) can also be a powerful tool for application in understanding the thermochemistry of clay calcination, although also come with some disadvantages when approaching calculations on such complex (often disordered) layered structures. Even the analysis of uncalcined clay minerals by DFT can be controversial, with differences between published studies on fundamental aspects of space groups, bond lengths and orientations for a mineral as well-known as pure, highly-crystalline kaolinite.[63,64] More complex structures such as halloysite[65] and Fe-substituted kaolinite,[66] as well as the role of stacking faults in kaolinite,[67] have also been studied with some success by density functional techniques. The importance of correct application of high-level theory including appropriate corrections for dispersion and other physicochemical phenomena has particularly been highlighted.[68–70] Much of the literature in this field has been focused on determining surface interactions between kaolinite and other molecules, although exfoliation (which is a process of interest with respect to cementitious reactivity) and small-molecule intercalation have also been considered in a number of studies.[70–72]

Calcination of kaolinite has been described using a stepwise DFT approach,[73] progressively removing hydroxyl groups and allowing the structure to relax, in simulations that were intended to describe the thermally induced dehydroxylation process during calcination. Fig. 14 shows the progressive disordering and layer disruption induced by this stepwise process, as simulated by White *et al.*[73]. Izadifar *et al.*[51] have also addressed this question for dehydroxylation of both kaolinite and dickite,

and provided description of their results in terms of the chemical potential of water accompanying each structure, which is an alternative and potentially very valuable approach to representing data of this type.

Detailed work has also highlighted the importance of correct relaxation of atom positions in structure determination of disordered structures such as that of metakaolin to ensure chemical plausibility of the structural model,[74] and conversely also the importance of incorporation of experimental data into computational approaches to ensure realistic outcomes.[74,75] Fundamentally, the structures of dehydroxylated clays are sufficiently complex that application of a pure theoretical approach, or a pure experimental approach without reference to theory, in determination of their structures and thermochemistry is unlikely to succeed in the absence of rigorous validation. Important advances have recently been made in related areas, including simulations of the aqueous dissolution of clay minerals[76] and in the application of force-field methods to cement hydrates and hydration.[77] It appears likely that future developments in theory and applications will also lead to improvements in how clay calcination processes and products are understood from this fundamental level.

Modeling the reaction of calcined clays in cementitious binders

The understanding of cement hydration is much older than the application of thermodynamic modeling to cementitious binders, which has been gaining major attention in the last few decades.[78–82] Several approaches (Table 5) have been developed with different levels of detail and therefore varying modeling
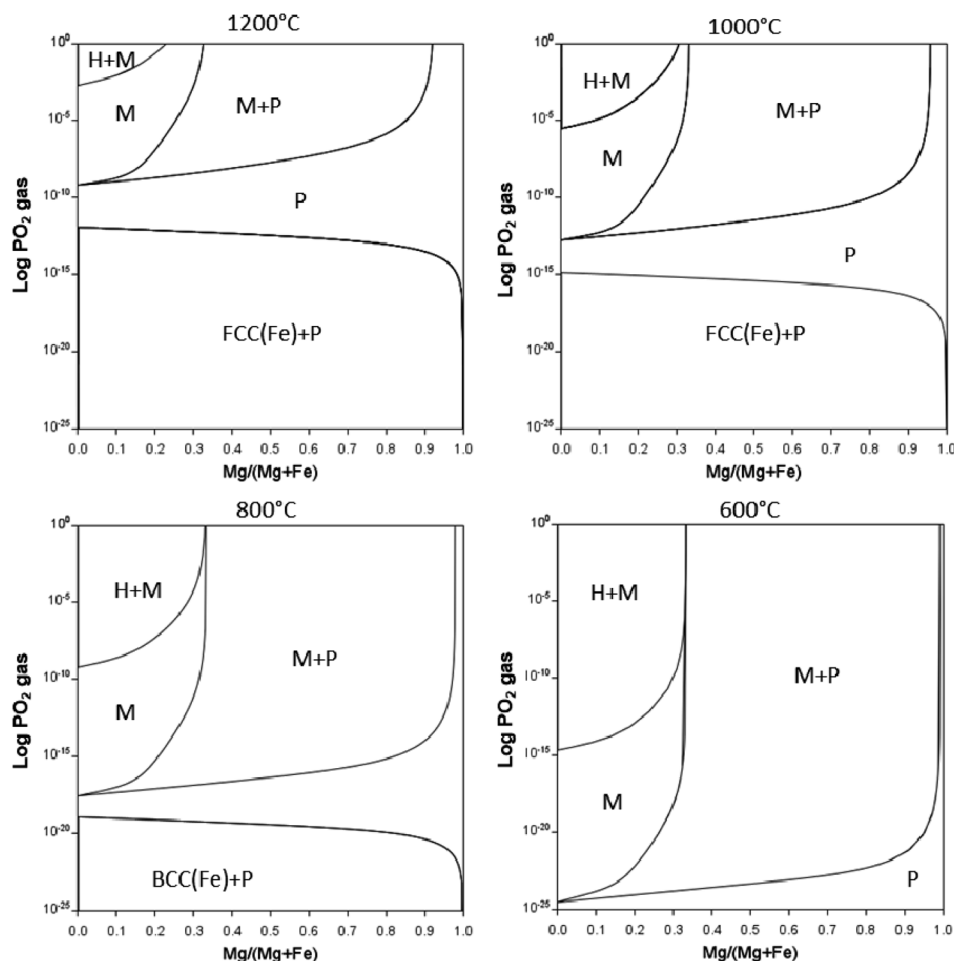
17930 | *J. Mater. Chem. A*, 2023, **11**, 17920–17937

This journal is © The Royal Society of Chemistry 2023

Fig. 13 Mg/(Mg + Fe) *vs.* activity of log P_{O_2} in gas at 1200, 1000, 800 and 600 °C where M = magnetite (Fe,Mg)$_3$O$_4$, H = hematite (Fe$_2$O$_3$), P = periclase (Fe,Mg)O calculated using Thermo-Calc software TCOX Metal Slag and Oxides Database version 11.

input data requirements which can be categorized in the following strategies.

These modeling approaches can also be combined. For example, one may choose to let fast reacting phases react in an unconstrained manner (full hydration) while reducing the reaction of slowly reacting phases such as belite to approximate the hydration of the binder of interest. Often the hydration kinetics makes the difference between good and poor modeling, based on agreement between the predicted and observed hydrate phases.[83]

For the hydration of calcined clays, one should distinguish several main binder categories (I) 'model' systems activated by lime or alkaline solutions, (II) binary,[91] and (III) ternary binders containing Portland cement. The latter binders contain, in most cases, limestone filler, due to the commercial and environmental benefits of these materials[92] and standards which allow replacement. Those ternary binders are often, but not necessarily, labelled as LC^3-type binders.[93] The addition of limestone filler produces stable phase assemblages in which the ettringite is stabilized and the reactive aluminium is incorporated in C–A–S–H and mono- or hemi- carboaluminate AFm phases over a wide range of compositions and clay types.[83] Thermodynamically, monocarbonate is often predicted while hemicarbonate

may be observed initially, which may be due to kinetics or anion availability. In any case, the solubility of both phases are quite close to each other;[6] therefore, small variances may make the difference between the phases observed and predicted. Another feature of these binders for high clay replacement levels is the predicted precipitation of strätlingite in the absence of portlandite, while in experiments often traces of portlandite are still present when strätlingite is observed also, which should not be the case based on thermodynamic modeling and is often explained through either kinetic effects or lack of ionic transport in very fine pore systems.[88,94] Binders (III) with low limestone content may display a larger variety of members from the AFm phase family including strätlingite.[83] These binders can show phase assemblages closer to binary blends (II), where the calcium sulphate content also plays a crucial role in the resulting phase assemblages.

The challenges that arise for modeling of both binary and ternary binders is to gather the dissolution rates (kinetic) of the calcined clay fraction which may differ due to:

- The chemical and mineralogical composition (including impurities) of the starting material.
- Physical properties of the starting material (particle size, surface areas, *etc.*).
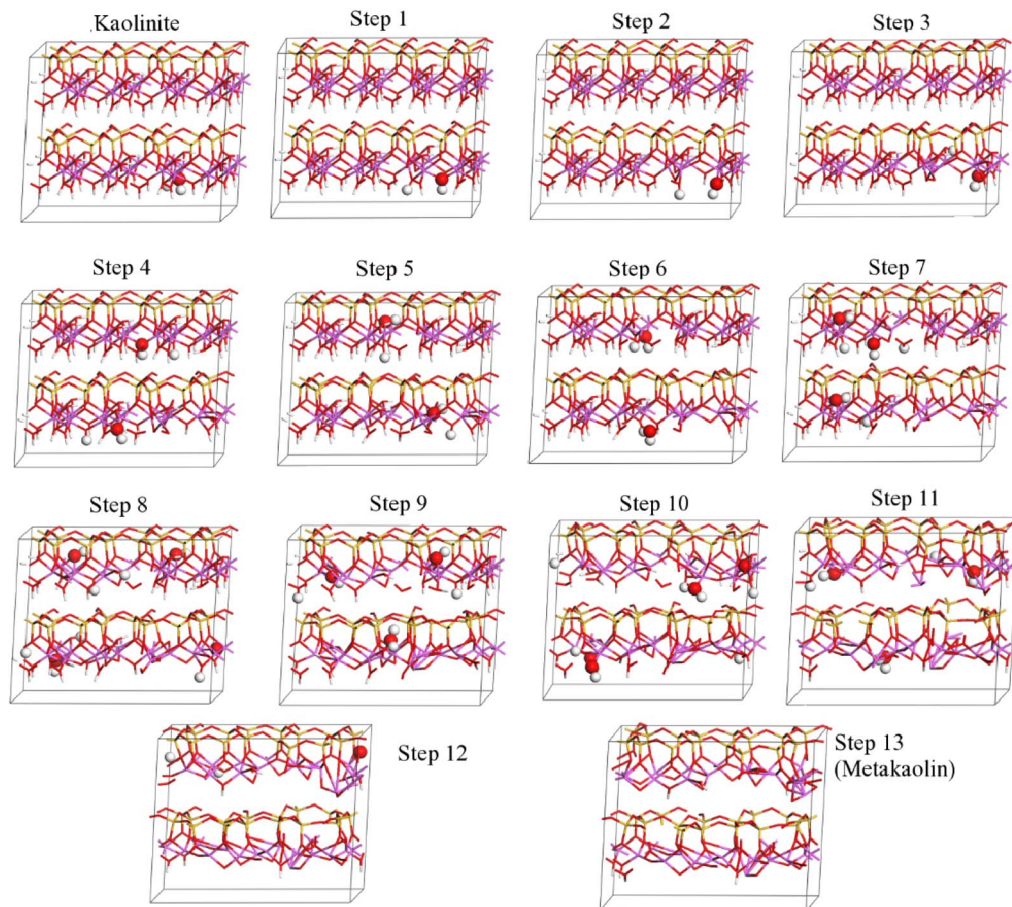
This journal is © The Royal Society of Chemistry 2023

J. Mater. Chem. A, 2023, **11**, 17920–17937 | **17931**

Fig. 14 Stepwise dehydroxylation of a kaolinite supercell to metakaolin, as calculated by DFT.[73] In that study, the kaolinite model was found to describe the experimentally observed structures (from neutron and X-ray pair distribution functions) for calcination temperatures up to 450 °C; step 9 corresponded to 500 °C, step 12 to 550 °C, and step 13 to 750 °C. The enlarged atoms in each structural model indicate the hydroxyl groups removed in the subsequent step. Reproduced from ref. 73 with permission from American Chemical Society, copyright 2010.

- The calcination process (temperature, retention time, atmosphere, heating and cooling rates, *etc.*).
- Type of the cement used for activation.
- Mixture proportion (clay, limestone and gypsum quantities).

Results from such tests have been used for modeling and classification of clays.[83,94,95]

The binders labelled above as model systems[96] (I) represent a range of systems that range from reactivity tests when activated on small scales[97,98] and as hydraulic lime-pozzolana mortars based on local alternatives to industrial cementitious binders.[99,100] The focus here will be placed on cement-based binders. Interested readers are referred to suitable review papers for alkaline activated binders on this topic.[101,102]

While the nature of most kinetic models used in thermodynamic modeling has an empirical component, there is the desire in the research community to link these measurable

Table 5 Common modeling approaches to describe cement hydration with/without SCMs and the required input parameters/boundary conditions

Modeling approach	Water/binder ratio	Chemical composition	Mineralogical composition	Hydration degree	Hydration kinetics	References
Full hydration	×	×				83–86
Partial cement hydration	×	×		×		87 and 88
Clinker (+SCM) phase separated hydration degrees	×	×	×	×		89 and 90
Implementation of hydration kinetics	×	×	×		×	80 and 83

"macro" scale effects to scientific questions on smaller scales, like the dissolution rate which may be complicated by solid solutions of clays utilised in practice. However, while there is no lack of literature on the dissolution of pure clay minerals in the geochemical domain, there are only a few articles tackling this topic for specifically metakaolin in acidic environments or alkali activated binders.[103–107]

Property and performance prediction

The motivation for the use of thermodynamic modeling is often driven by the attempt to understand underlying material chemistry and link/predict phase development and the durability of binders without decades of testing. Examples of this for calcined clay binders include the comparison of calculated porosity and mechanical properties as shown in Fig. 15. Kunther et al.[108] showed that relationships between compressive strength and calculated porosity follow similar trends as described by empirical models such as the Ryshkewitch model.[109]

These types of calculations provide, especially for similar cement blends, qualitative relationships that appear appropriate. While these relationships may seem intuitive, the comparison between two binders, for example with two different clays and equal replacement rates, can highlight limitations because the same porosity may yield two compressive strengths. Such differences can be explained by changes in mineralogy, reactivity, and replacement of the materials. Other applications could be:

- Estimates for permeable pore spaces or.
- Identification of key minerals relevant for durability assessments.[110–112]

We do not know all relevant material parameters: the compressive strength of composite materials, where the relevant parameters include the porosity (larger pores are more

Fig. 15 Comparison of the measured compressive strength of mortar bars and the calculated porosity changes during hydration[108] based on kinetic inputs.[83] The mineralogical compositions were for clay 1: 23% illite, 4% kaolinite, 36% quartz, 1% calcite, 36% amorphous and for clay 2: 48% illite, 5% kaolinite, 8% quartz, 43% amorphous.

critical), hydrate phase assemblage including Ca/Si ratio of the C–A–S–H phases, mechanical properties of individual and solid-solutions of hydrate minerals, microstructural features (through homogenization schemes), and impact of other inclusions. It is not a simple task to predict conventional mechanical properties based on the chemistry and kinetics alone. One step forward is therefore to model also the micro-structure, as has been proposed by reactive transport models;[113] not all the pore space calculated in thermodynamic models is accessible for ionic liquids and thus the permeable volume will be smaller than the predicted volume.

Durability modeling of calcined clay binders is documented in a few studies only,[110,112] as a recent review of the durability of binary and ternary binders also supported.[114] However, the presented results suggest that the general processes identified. e.g. for carbonation, chloride binding, or sulfate attack will also apply to these binders as long as the phase assemblages are similar in terms of portlandite content, Ca/Si ratio of C–A–S–H phases, and presence of AFm phases, which might be similar to fly ash containing Portland cements (typically 6–35 wt% replacement) and higher replacement slag cements. Hence, one needs to understand the limitations of modeling in context with the expected service environment in order to be able to assess possible durability issues which are affected by the clay reactivity in combination with the chosen cement type and resulting phase assemblage. Additionally, durability issues that are not directly related to the clay properties, such as alkali–silica reaction or frost, may provide additional stressors that may shorten the service life when occurring simultaneously. In summary, a lack of modeling knowledge on durability is apparent.

Concluding remarks

The variety of input data of raw clays, due to solid solutions and physical mixtures of sediment deposits, is large. This requires extensive understanding of the processes to activate and utilize the clays in construction materials. Calcination depends on the minerals present which may impose compromise to achieve maximum reactivity, but relevant thermodynamic data, in particular for metastable/reactive clay phases, is lacking. Several parameters are not yet experimentally verified but modeling attempts have been initiated. There is an apparent lack of models for calcination processes that link the theoretical calculations with process parameters in the publicly available literature, and future work should focus on experimentally assessing the influence of process atmosphere on calcined clay production and quality. The use of inorganic modifiers to stabilise magnetite at low temperature can also be predicted through thermodynamic modeling and the processing of raw clays from one type to another is an unexplored avenue that must be investigated.

As highlighted in this article, there are plenty data sources to draw from and information are available when it comes to the hydration of cementitious binders containing calcined clays; other binder types might display similar phase assemblages and synergies such as ternary binders containing fly ash and
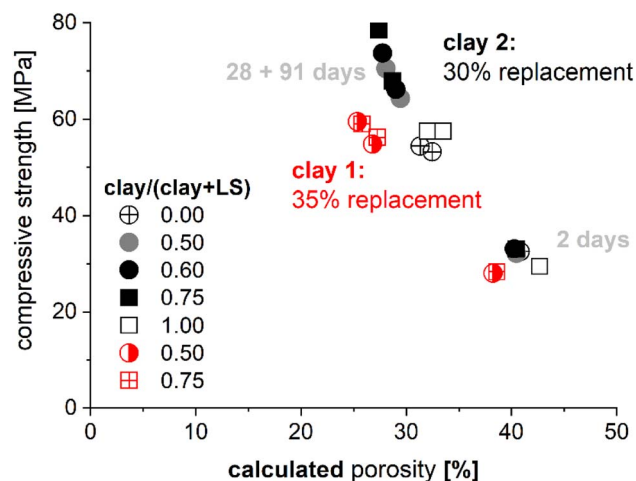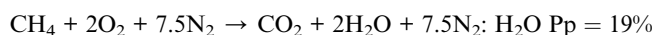
limestone fillers.[115] An aspect that is not well established is the interplay between different cements also within the same cement class in relation to blended binary or ternary cements even though some studies have documented some results already.[116] The same will also be valid for alternative activators.

Microstructure differences will arise in new cements. Additionally, the measurement of porosity and permeability has a long-lasting history when it comes to the applicability, sample preparation, and comparison between different measurement methods and sample preparation in concrete technology and cement science.[117,118] All these aspects become important when it comes to the estimation of the service life.
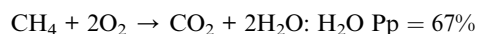
Due to the underdeveloped understanding of *ab initio* prediction of the dissolution of powders of mixtures of minerals with a range of particle sizes, or pyro processing conditions to obtain highly reactive calcined clays as SCMs, this is a topic that requires further exploration. Similarly, the experimental derivation of thermodynamic data that can be achieved using advanced calorimetric and/or dissolution techniques is necessary for co-validation.
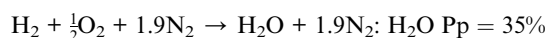
Appendix

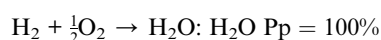The combustion of simple fossil fuel (methane) in stoichiometric air (assuming air is 79% V N_2 and 21% V O_2).

$$CH_4 + 2O_2 + 7.5N_2 \rightarrow CO_2 + 2H_2O + 7.5N_2: H_2O \; Pp = 19\%$$

Oxyfuel combustion of simple fossil fuel (methane):

$$CH_4 + 2O_2 \rightarrow CO_2 + 2H_2O: H_2O \; Pp = 67\%$$

The combustion of hydrogen gas in stoichiometric air (assuming air is 79% V N_2 and 21% V O_2).

$$H_2 + \tfrac{1}{2}O_2 + 1.9N_2 \rightarrow H_2O + 1.9N_2: H_2O \; Pp = 35\%$$

Oxyfuel combustion of hydrogen gas:

$$H_2 + \tfrac{1}{2}O_2 \rightarrow H_2O: H_2O \; Pp = 100\%$$

Conflicts of interest

There are no conflicts to declare.

Acknowledgements

References

1 U.S. Geological Survey, *Mineral Commodity Summaries*, National Minerals Information Center, 2022, https://www.usgs.gov/centers/national-minerals-information-center/cement-statistics-and-information.

2 K. Scrivener, *et al.*, Calcined clay limestone cements (LC3), *Cem. Concr. Res.*, 2018, **114**, 49–56.

3 D. A. Kulik, *et al.*, CemGEMS–an easy-to-use web application for thermodynamic modelling of cementitious materials, *RILEM Tech. Lett.*, 2021, **6**, 36–52.

4 G. D. Miron, S. Dmytrieva and D. A. Kulik, ThermoFun: A C++/Python library for computing standard thermodynamic properties of substances and reactions across wide ranges of temperatures and pressures, *J. Open Source Softw.*, 2023, **8**(83), 4624.

5 H. Le Chatelier, *Experimental Researches on the Constitution of Hydraulic Mortars*, McGraw Publishing Company, 1905.

6 B. Lothenbach, *et al.*, Cemdata18: A chemical thermodynamic database for hydrated Portland cements and alkali-activated materials, *Cem. Concr. Res.*, 2019, **115**, 472–506.

7 T. Hanein, F. P. Glasser and M. N. Bannerman, Thermodynamic data for cement clinkering, *Cem. Concr. Res.*, 2020, **132**, 106043.

8 S. Ghazizadeh, *et al.*, Estimation of standard molar entropy of cement hydrates and clinker minerals, *Cem. Concr. Res.*, 2020, **136**, 106188.

9 T. Hanein, *et al.*, Clay calcination technology: state-of-the-art review by the RILEM TC 282-CCL, *Mater. Struct.*, 2022, **55**(3), 1–29.

10 A. Z. Khalifa, *et al.*, Advances in alkali-activation of clay minerals, *Cem. Concr. Res.*, 2020, **132**, 106050.

11 J. L. Provis, Alkali-activated materials, *Cem. Concr. Res.*, 2018, **114**, 40–48.

12 I. H. Shah, *et al.*, Cement substitution with secondary materials can reduce annual global CO_2 emissions by up to 1.3 gigatons, *Nat. Commun.*, 2022, **13**(1), 5758.

13 minteq.v4.dat: The minteq.v4.dat database. in phreeqc: R Interface to Geochemical Modeling Software, https://rdrr.io/cran/phreeqc/man/minteq.v4.dat.html.

14 *PHREEQC Version 3*, 2021, https://www.usgs.gov/software/phreeqc-version-3.

15 J. Johnson, F. Anderson and D. Parkhurst, *Database thermo.com.V8.R6.230, Rev 1.11*, Lawrence Livermore National Laboratory, Livermore, California, 2000.

16 C. E. A. Palmer, R. J. Silva and J. J. Bucher, *Thermodynamic Data Base Needs for Modeling Studies of the Yucca Mountain Project*, Citeseer, 1996.

17 P. Blanc, *et al.*, Thermoddem: A geochemical database focused on low temperature water/rock interactions and waste materials, *Appl. Geochem.*, 2012, **27**(10), 2107–2116.

18 Thermoddem, Thermochemical and Mineralogical Tables for Geochemical Modeling: https://thermoddem.brgm.fr/databases/phreeqc.

19 L. Duro, M. Grivé and E. Giffaut, *ThermoChimie, the ANDRA Thermodynamic Database*, MRS Online Proceedings Library (OPL), 2012, vol. 1475.

20 E. Giffaut, *et al.*, Andra thermodynamic database for performance assessment: ThermoChimie, *Appl. Geochem.*, 2014, **49**, 225–236.

21 NEA, *Thermochemical Database (TDB) Project*, https://www.oecd-nea.org/jcms/pl_22166/thermochemical-database-tdb-project.

22 JAEA, *Thermodynamic Database for Nuclear Fuels and Reactor Materials*, https://thermodb.jaea.go.jp/en/db/index.html.

23 T. J. B. Holland and R. Powell, An improved and extended internally consistent thermodynamic dataset for phases of petrological interest, involving a new equation of state for solids, *J. Metamorph. Geol.*, 2011, **29**(3), 333–383.

24 Y. Tardy and B. Fritz, An ideal solid solution model for calculating solubility of clay minerals, *Clay Miner.*, 1981, **16**(4), 361–373.

25 B. Fritz, Multicomponent solid solutions for clay minerals and computer modeling of weathering processes, in *The Chemistry of Weathering*, Springer, 1985, pp. 19–34.

26 P. Aagaard and H. C. Helgeson, Activity/composition relations among silicates and aqueous solutions: II. Chemical and thermodynamic consequences of ideal mixing of atoms on homological sites in montmorillonites, illites, and mixed-layer clays, *Clays Clay Miner.*, 1983, **31**(3), 207–217.

27 W. F. Giggenbach, Construction of thermodynamic stability diagrams involving dioctahedral potassium clay minerals, *Chem. Geol.*, 1985, **49**(1–3), 231–242.

28 M. F. Brigatti, E. Galan, and B. K. G. Theng, Structure and mineralogy of clay minerals, in *Developments in Clay Science*, Elsevier, 2013, pp. 21–81.

29 G. W. Brindley and R. Wardle, Monoclinic and triclinic forms of pyrophyllite and pyrophyllite anhydride, *Am. Mineral.*, 1970, **55**(7–8), 1259–1272.

30 E. Molina-Montes, *et al.*, DFT research on the dehydroxylation reaction of pyrophyllite 1. First-principle molecular dynamics simulations, *J. Phys. Chem. B*, 2008, **112**(23), 7051–7060.

31 J. J. Fitzgerald, *et al.*, Solid-State 27 Al and 29 Si NMR and H CRAMPS Studies of the Thermal Transformations of the 2:1 Phyllosilicate Pyrophyllite, *J. Phys. Chem.*, 1996, **100**(43), 17351–17360.

32 V. A. Drits, A. Derkowski and D. K. McCarty, Kinetics of thermal transformation of partially dehydroxylated pyrophyllite, *Am. Mineral.*, 2011, **96**(7), 1054–1069.

33 O. Vidal and B. Dubacq, Thermodynamic modelling of clay dehydration, stability and compositional evolution with temperature, pressure and H_2O activity, *Geochim. Cosmochim. Acta*, 2009, **73**(21), 6544–6564.

34 P. Blanc, *et al.*, Thermodynamics for clay minerals: Calculation tools and application to the case of illite/smectite interstratified minerals, *Appl. Geochem.*, 2021, **130**, 104986.

35 P. Blanc, *et al.*, A generalized model for predicting the thermodynamic properties of clay minerals, *Am. J. Sci.*, 2015, **315**(8), 734–780.

36 H. Gailhanou, *et al.*, Methodology for determining the thermodynamic properties of smectite hydration, *Appl. Geochem.*, 2017, **82**, 146–163.

37 P. Vieillard, *et al.*, A predictive model of thermodynamic entities of hydration for smectites: Application to the formation properties of smectites, *Appl. Geochem.*, 2019, **110**, 104423.

38 H. D. B. Jenkins and L. Glasser, Standard absolute entropy, values from volume or density. 1. inorganic materials, *Inorg. Chem.*, 2003, **42**(26), 8702–8708.

39 J. Leitner, *et al.*, Application of Neumann–Kopp rule for the estimation of heat capacity of mixed oxides, *Thermochim. Acta*, 2010, **497**(1–2), 7–13.

40 H. Kopp, XX.—Investigations of the specific heat of solid bodies, *J. Chem. Soc.*, 1866, **19**, 154–234.

41 R. A. Robie and B. S. Hemingway, *Thermodynamic Properties of Minerals and Related Substances at 298.15 K and 1 Bar (10^5 Pascals) Pressure and at Higher Temperatures*, 1995.

42 G. Grimvall, *Thermophysical Properties of Materials*, Elsevier, 1999.

43 C. E. White, *et al.*, Inelastic neutron scattering analysis of the thermal decomposition of kaolinite to metakaolin, *Chem. Phys.*, 2013, **427**, 82–86.

44 F. Zunino, E. Boehm-Courjault and K. Scrivener, The impact of calcite impurities in clays containing kaolinite on their reactivity in cement after calcination, *Mater. Struct.*, 2020, **53**, 44.

45 T. Danner, *et al.*, Feasibility of calcined marl as an alternative pozzolanic material, in *Calcined Clays for Sustainable Concrete*, Springer, 2015, pp. 67–73.

46 T. A. Østnor and H. Justnes, Durability of mortar with calcined marl as supplementary cementing material, *Adv. Cem. Res.*, 2014, **26**(6), 344–352.

47 T. Hanein, *et al.*, Production of belite calcium sulfoaluminate cement using sulfur as a fuel and as a source of clinker sulfur trioxide: pilot kiln trial, *Adv. Cem. Res.*, 2016, **28**(10), 643–653.

48 T. Hanein, *et al.*, Stability of ternesite and the production at scale of ternesite-based clinkers, *Cem. Concr. Res.*, 2017, **98**(C), 91–100.

49 N. C. Schieltz and M. R. Soliman, Thermodynamics of the various high temperature transformations of kaolinite, *Clays Clay Miner.*, 1964, **13**(1), 419–428.

50 B. J. McBride, M. J. Zehe and S. Gordon, NASA Glenn coefficients for calculating thermodynamic properties of individual species, *National Aeronautics and Space Administration*, John H. Glenn Research Center at Lewis Field, 2002.

51 M. Izadifar, *et al.*, Comprehensive examination of dehydroxylation of kaolinite, disordered kaolinite, and dickite: Experimental studies and density functional theory, *Clays Clay Miner.*, 2020, **68**(4), 319–333.

52 J. L. Haas Jr, G. R. Robinson Jr and B. S. Hemingway, Thermodynamic tabulations for selected phases in the

This journal is © The Royal Society of Chemistry 2023

J. Mater. Chem. A, 2023, **11**, 17920–17937 | **17935**

system $CaO-Al_2O_3-SiO_2-H_2$ at 101.325 kPa (1 atm) between 273.15 and 1800 K, *J. Phys. Chem. Ref. Data*, 1981, **10**(3), 575–670.

53 M. Zajac, *et al.*, Effect of hydration kinetics on properties of compositionally similar binders, *Cem. Concr. Res.*, 2017, **101**, 13–24.

54 H. Blatt, G. V. Middleton and R. C. Murray, *Origin of Sedimentary Rocks.* 1972.

55 E. Galán, Genesis of clay minerals, *Dev. Clay Sci.*, 2006, **1**, 1129–1162.

56 A. Alujas Diaz, R. S. Almenares Reyes, T. Hanein, E. F. Irassar, M. Juenger, F. Kanavaris, M. Maier, A. T. Marsh, T. Sui, K. C. Thienel and L. Valentini, Properties and occurrence of clay resources for use as supplementary cementitious materials: a paper of RILEM TC 282-CCL, *Mater. Struct.*, 2022, **55**(5), 139, under review.

57 A. Ito and R. Wagai, Global distribution of clay-size minerals on land surface for biogeochemical and climatological studies, *Sci. Data*, 2017, **4**, 170103.

58 J. F. Martirena Hernandez, *et al.*, Color control in industrial clay calcination, *RILEM Tech. Lett.*, 2020, **5**, 1–7.

59 Thermo-Calc software TCOX Metal Slag and Oxides Database version 11, **https://thermocalc.com/products/databases/metal-oxide-solutions/**, accessed 16 November 2022.

60 X. Liang, *et al.*, The influence of substituting metals (Ti, V, Cr, Mn, Co and Ni) on the thermal stability of magnetite, *J. Therm. Anal. Calorim.*, 2013, **111**(2), 1317–1324.

61 A. U. Seybolt, Observations on the Fe-Cr-O System, *J. Electrochem. Soc.*, 1960, **107**(3), 147.

62 V. Raghavan, Fe-Mg-O (Iron-Magnesium-Oxygen), *J. Phase Equilib. Diffus.*, 2010, **31**(4), 368.

63 X. L. Hu and A. Michaelides, Water on the hydroxylated (0 0 1) surface of kaolinite: From monomer adsorption to a flat 2D wetting layer, *Surf. Sci.*, 2008, **602**(4), 960–974.

64 C. E. White, *et al.*, What is the structure of kaolinite? Reconciling theory and experiment, *J. Phys. Chem. B*, 2009, **113**(19), 6756–6765.

65 F. Ferrante, N. Armata and G. Lazzara, Modeling of the halloysite spiral nanotube, *J. Phys. Chem. C*, 2015, **119**(29), 16700–16707.

66 D. Richard and N. M. Rendtorff, Local environments in iron-bearing clay minerals by DFT approaches: the case of structural Fe in kaolinite, *Appl. Clay Sci.*, 2021, **213**, 106251.

67 C. E. White, *et al.*, Structure of kaolinite and influence of stacking faults: reconciling theory and experiment using inelastic neutron scattering analysis, *J. Chem. Phys.*, 2013, **138**(19), 194501.

68 D. Tunega, T. Bučko and A. Zaoui, Assessment of ten DFT methods in predicting structures of sheet silicates: Importance of dispersion corrections, *J. Chem. Phys.*, 2012, **137**(11), 114105.

69 P. F. Weck, E. Kim and C. F. Jové-Colón, Relationship between crystal structure and thermo-mechanical properties of kaolinite clay: beyond standard density functional theory, *Dalton Trans.*, 2015, **44**(28), 12550–12560.

70 M. Cutini, L. Maschio and P. Ugliengo, Exfoliation energy of layered materials by DFT-D: Beware of dispersion!, *J. Chem. Theory Comput.*, 2020, **16**(8), 5244–5252.

71 C. E. White, *et al.*, Effect of temperature on the local structure of kaolinite intercalated with potassium acetate, *Chem. Mater.*, 2011, **23**(2), 188–199.

72 J. Wang, *et al.*, Energetics, interlayer molecular structures, and hydration mechanisms of dimethyl sulfoxide (DMSO)–kaolinite nanoclay guest–host interactions, *J. Phys. Chem. Lett.*, 2021, **12**(40), 9973–9981.

73 C. E. White, *et al.*, Density functional modeling of the local structure of kaolinite subjected to thermal dehydroxylation, *J. Phys. Chem. A*, 2010, **114**(14), 4988–4996.

74 C. E. White, *et al.*, Combining density functional theory (DFT) and pair distribution function (PDF) analysis to solve the structure of metastable materials: the case of metakaolin, *Phys. Chem. Chem. Phys.*, 2010, **12**(13), 3239–3245.

75 I. G. Richardson, The importance of proper crystal-chemical and geometrical reasoning demonstrated using layered single and double hydroxides, *Acta Crystallogr., Sect. B: Struct. Sci., Cryst. Eng. Mater.*, 2013, **69**(2), 150–162.

76 R. Schliemann and S. V. Churakov, Atomic scale mechanism of clay minerals dissolution revealed by ab initio simulations, *Geochim. Cosmochim. Acta*, 2021, **293**, 438–460.

77 R. K. Mishra, *et al.*, cemff: A force field database for cementitious materials including validations, applications and opportunities, *Cem. Concr. Res.*, 2017, **102**, 68–89.

78 E. M. Gartner and H. M. Jennings, Thermodynamics of calcium silicate hydrates and their solutions, *J. Am. Ceram. Soc.*, 1987, **70**(10), 743–749.

79 P. Hewlett and M. Liska, *Lea's Chemistry of Cement and Concrete*, Butterworth-Heinemann, 2019.

80 B. Lothenbach and F. Winnefeld, Thermodynamic modelling of the hydration of Portland cement, *Cem. Concr. Res.*, 2006, **36**(2), 209–226.

81 D. Damidot, *et al.*, Thermodynamics and cement science, *Cem. Concr. Res.*, 2011, **41**(7), 679–695.

82 B. Lothenbach and M. Zajac, Application of thermodynamic modelling to hydrated cements, *Cem. Concr. Res.*, 2019, **123**, 105779.

83 W. Kunther, Z. Dai and J. Skibsted, Thermodynamic modeling of hydrated white Portland cement–metakaolin–limestone blends utilizing hydration kinetics from 29Si MAS NMR spectroscopy, *Cem. Concr. Res.*, 2016, **86**, 29–41.

84 A. Machner, *et al.*, Portland metakaolin cement containing dolomite or limestone–Similarities and differences in phase assemblage and compressive strength, *Constr. Build. Mater.*, 2017, **157**, 214–225.

85 G. Puerta-Falla, *et al.*, The influence of metakaolin on limestone reactivity in cementitious materials, in *Calcined Clays for Sustainable Concrete*, Springer, 2015, pp. 11–19.

86 N. Chitvoranund, *et al.*, Reactivity of Calcined Clay in Alite-Calcium Sulfoaluminate Cement Hydration, in *Calcined Clays for Sustainable Concrete*, Springer, 2015, pp. 373–379.

17936 | *J. Mater. Chem. A*, 2023, **11**, 17920–17937

This journal is © The Royal Society of Chemistry 2023

87 K. De Weerdt, H. Justnes and M. R. Geiker, Changes in the phase assemblage of concrete exposed to sea water, *Cem. Concr. Compos.*, 2014, **47**, 53–63.

88 M. Antoni, *et al.*, Cement substitution by a combination of metakaolin and limestone, *Cem. Concr. Res.*, 2012, **42**(12), 1579–1589.

89 M. Pedersen, *et al.*, Hydrate phase assemblages in calcium sulfoaluminate–metakaolin–limestone blends, in *Calcined Clays for Sustainable Concrete*, Springer, 2018, pp. 352–357.

90 F. Avet and K. Scrivener, Reaction degree of metakaolin in limestone calcined clay cement (LC 3), in *Calcined Clays for Sustainable Concrete*, Springer, 2018, pp. 41–45.

91 P. Duan, *et al.*, Influence of metakaolin on pore structure-related properties and thermodynamic stability of hydrate phases of concrete in seawater environment, *Constr. Build. Mater.*, 2012, **36**, 947–953.

92 K. L. Scrivener, V. M. John and E. M. Gartner, Eco-efficient cements: Potential economically viable solutions for a low-CO_2 cement-based materials industry, *Cem. Concr. Res.*, 2018, **114**, 2–26.

93 F. Zunino, F. Martirena and K. Scrivener, Limestone calcined clay cements (LC³), *ACI Mater. J.*, 2021, **118**(3), 49–60.

94 K. E. Rasmussen, *et al.*, Comparison of the pozzolanic reactivity for flash and soak calcined clays in Portland cement blends, in *Calcined Clays for Sustainable Concrete*, Springer, 2015, pp. 151–157.

95 J. Skibsted and R. Snellings, Reactivity of supplementary cementitious materials (SCMs) in cement blends, *Cem. Concr. Res.*, 2019, **124**, 105799.

96 N. Garg and J. Skibsted, Dissolution kinetics of calcined kaolinite and montmorillonite in alkaline conditions: Evidence for reactive Al (V) sites, *J. Am. Ceram. Soc.*, 2019, **102**(12), 7720–7734.

97 J. Ninov, *et al.*, On the kinetics of pozzolanic reaction in metakaolin–lime–water system, *J. Therm. Anal. Calorim.*, 2011, **105**(1), 245–250.

98 I. Dojkov, *et al.*, On the consumption of lime by metakaolin, fly ash and kaoline in model systems, *J. Chem. Technol. Metall.*, 2013, **48**(1), 54–60.

99 C. Shi and R. L. Day, Chemical activation of blended cements made with lime and natural pozzolans, *Cem. Concr. Res.*, 1993, **23**(6), 1389–1396.

100 J. I. Alvarez, *et al.*, RILEM TC 277-LHS report: A review on the mechanisms of setting and hardening of lime-based binding systems, *Mater. Struct.*, 2021, **54**(2), 1–30.

101 J. L. Provis, *et al.*, Binder chemistry–Low-calcium alkali-activated materials, in *Alkali Activated Materials*, Springer, 2014, pp. 93–123.

102 J. J. Jeremiah, *et al.*, Geopolymers as alternative sustainable binders for stabilisation of clays—a review, *Geotechnics*, 2021, **1**(2), 439–459.

103 L. Valentini, Modeling dissolution–precipitation kinetics of alkali-activated metakaolin, *ACS Omega*, 2018, **3**(12), 18100–18108.

104 C. E. White, *et al.*, Molecular mechanisms responsible for the structural changes occurring during geopolymerization: multiscale simulation, *AIChE J.*, 2012, **58**(7), 2241–2253.

105 A. Hajimohammadi and J. S. J. van Deventer, Dissolution behaviour of source materials for synthesis of geopolymer binders: A kinetic approach, *Int. J. Miner. Process.*, 2016, **153**, 80–86.

106 D. K. Saleh, *et al.*, Dissolution of aluminium from metakaolin with oxalic, citric and lactic acids, *Clay Miner.*, 2019, **54**(2), 209–217.

107 P. E. A. Lima, R. S. Angélica and R. F. Neves, Dissolution kinetics of metakaolin in sulfuric acid: comparison between heterogeneous and homogeneous reaction methods, *Appl. Clay Sci.*, 2014, **88**, 159–162.

108 W. Kunther, *et al.*, Evaluation of the compressive strength for Portland cement blends incorporating real calcined clays and limestone by thermodynamic modeling, in *2nd International Conference on the Chemistry of Construction Materials (ICCCM 2016)*, Munich, Germany, 2016, p. 4.

109 E. Ryshkewitch, Compression strength of porous sintered alumina and zirconia: 9th communication to ceramography, *J. Am. Ceram. Soc.*, 1953, **36**(2), 65–68.

110 Z. Shi, *et al.*, Friedel's salt profiles from thermogravimetric analysis and thermodynamic modelling of Portland cement-based mortars exposed to sodium chloride solution, *Cem. Concr. Compos.*, 2017, **78**, 73–83.

111 V. Shah, *et al.*, Changes in microstructure characteristics of cement paste on carbonation, *Cem. Concr. Res.*, 2018, **109**, 184–197.

112 Z. Shi, *et al.*, Experimental studies and thermodynamic modeling of the carbonation of Portland cement, metakaolin and limestone mortars, *Cem. Concr. Res.*, 2016, **88**, 60–72.

113 A. Michel, *et al.*, Microstructural changes and mass transport in cement-based materials: A modeling approach, *Cem. Concr. Res.*, 2021, **139**, 106285.

114 Y. Dhandapani, *et al.*, Durability performance of binary and ternary blended cementitious systems with calcined clay: a RILEM TC 282 CCL review, *Mater. Struct.*, 2022, **55**(5), 145.

115 K. De Weerdt, *et al.*, Synergy between fly ash and limestone powder in ternary cements, *Cem. Concr. Compos.*, 2011, **33**(1), 30–38.

116 M. Cyr, *et al.*, Effect of cement type on metakaolin efficiency, *Cem. Concr. Res.*, 2014, **64**, 63–72.

117 K. Scrivener, R. Snellings and B. Lothenbach, *A Practical Guide to Microstructural Analysis of Cementitious Materials*, CRC Press, 2018.

118 K. K. Aligizaki, *Pore Structure of Cement-Based Materials: Testing, Interpretation and Requirements*, CRC Press, 2005.

This journal is © The Royal Society of Chemistry 2023

J. Mater. Chem. A, 2023, **11**, 17920–17937 | **17937**